Inorg. Chem. **2005**, *44*, 4546–4554

X-ray Absorption Spectroscopic Study of the Reduced Hydroxylases of Methane Monooxygenase and Toluene/*o*-Xylene Monooxygenase: Differences in Active Site Structure and Effects of the Coupling Proteins MMOB and ToMOD

Deanne Jackson Rudd,[†] Matthew H. Sazinsky,[‡] Stephen J. Lippard,*[,‡] Britt Hedman,*[,§] and Keith O. Hodgson*[,†,§]

Departments of Chemistry, Stanford University, Stanford, California 94305, and Massachusetts Institute of Technology, Cambridge, Massachusetts 02139, and Stanford Synchrotron Radiation Laboratory, Stanford University, Stanford, California 94309

Received August 30, 2004

The diiron active sites of the reduced hydroxylases from methane monooxygenase ($MMOH_{red}$) and toluene/*o*-xylene monooxygenase ($ToMOH_{red}$) have been investigated by X-ray absorption spectroscopy (XAS). Results of Fe K-edge and extended X-ray absorption fine structure analysis reveal subtle differences between the hydroxylases that may be correlated to access of the active site. XAS data were also recorded for each hydroxylase in the presence of its respective coupling protein. MMOB affects the outer-shell scattering contributions in the diiron site of $MMOH_{red}$, whereas ToMOD exerts its main effect on the first-shell ligation of $ToMOH_{red}$; it also causes a slight decrease in the Fe–Fe separation. These results provide an initial step toward delineating the differences in structure and reactivity in bacterial multicomponent monooxygenase proteins.

Introduction

Bacterial multicomponent monooxygenases (BMMs) are capable of oxidizing a range of hydrocarbon-based substrates that are important in regulation of the global carbon cycle and of interest for bioremediation and industrial processes.[1,2] The best studied BMM is methane monooxygenase (MMO), which is the three-component protein system responsible for the conversion of methane to methanol as a source of energy in methanotrophic bacteria.[1,3] The hydroxylase (MMOH) contains a non-heme diiron active site where methanol is produced. MMOH is well characterized structurally and electronically, yet much is unknown about how this component interacts with the other proteins in the MMO system. MMOR is a [2Fe−2S]-containing reductase that is responsible for shuttling electrons from NADH to MMOH. MMOB, the "coupling" protein, contains neither metal centers nor cofactors, but forms a stable complex with MMOH that couples electron transfer with substrate hydroxylation.[1] MMOD,[4] a recently discovered fourth component, has an as yet unknown role, but recent X-ray absorption spectroscopy (XAS) investigations have shown that it has little effect on the structure of the active site in the oxidized form of MMOH.[5] Many studies have been performed to determine where and how these components bind to MMOH and, in particular, what effect MMOB has on the catalytic cycle.[6−14]

* Authors to whom correspondence should be addressed. E-mail: hodgson@ssrl.slac.stanford.edu (K.O.H.).
[†] Department of Chemistry, Stanford University.
[‡] Massachusetts Institute of Technology.
[§] Stanford Synchrotron Radiation Laboratory, Stanford University.

(1) Merkx, M.; Kopp, D. A.; Sazinsky, M. H.; Blazyk, J. L.; Müller, J.; Lippard, S. J. *Angew. Chem., Int. Ed.* **2001**, *40*, 2782−2807.
(2) Leahy, J. G.; Batchelor, P. J.; Morcomb, S. M. *FEMS Microbiol. Rev.* **2003**, *27*, 449−479.
(3) Waller, B. J.; Lipscomb, J. D. *Chem. Rev.* **1996**, *96*, 2625−2657.
(4) Merkx, M.; Lippard, S. J. *J. Biol. Chem.* **2002**, *277*, 5858−5865.
(5) Rudd, D. J.; Sazinsky, M. H.; Merkx, M.; Lippard, S. J.; Hedman, B.; Hodgson, K. O. *Inorg. Chem.* **2004**, *43*, 4579−4589.
(6) Gassner, G. T.; Lippard, S. J. *Biochemistry* **1999**, *38*, 12768−12785.
(7) DeWitt, J. G.; Rosenzweig, A. C.; Salifoglou, A.; Hedman, B.; Lippard, S. J.; Hodgson, K. O. *Inorg. Chem.* **1995**, *34*, 2505−2515.
(8) Walters, K. J.; Gassner, G. T.; Lippard, S. J.; Wagner, G. *Proc. Natl. Acad. Sci. U.S.A.* **1999**, *96*, 7877−7882.
(9) Brazeau, B. J.; Lipscomb, J. D. *Biochemistry* **2003**, *42*, 5618−5631.
(10) Pulver, S.; Froland, W. A.; Fox, B. G.; Lipscomb, J. D.; Solomon, E. I. *J. Am. Chem. Soc.* **1993**, *115*, 12409−12422.
(11) Pulver, S. C.; Froland, W. A.; Lipscomb, J. D.; Solomon, E. I. *J. Am. Chem. Soc.* **1997**, *119*, 387−395.
(12) Fox, B. G.; Liu, Y.; Dege, J. E.; Lipscomb, J. D. *J. Biol. Chem.* **1991**, *266*, 540−550.
(13) Wallar, B. J.; Lipscomb, J. D. *Biochemistry* **2001**, *40*, 2220−2233.
(14) Shu, L.; Liu, Y.; Lipscomb, J. D.; Que, L., Jr. *J. Biol. Inorg. Chem.* **1996**, *1*, 297−304.

10.1021/ic048794w CCC: $30.25
Published on Web 05/27/2005

When present in solution with MMOH, MMOR, NADH, and O_2, MMOB greatly increases the initial rate of enzyme turnover.[12] Furthermore, the high-valent intermediate $MMOH_Q$, which is the form of the protein that oxidizes methane, does not accumulate in the absence of substrate if MMOB is not present in the reaction mixture. This property is the result of a much slower reaction between fully reduced MMOH and O_2 to form the peroxo intermediate precursor to $MMOH_Q$.[15,16] Although MMOH has been crystallographically characterized in three oxidation states ($Fe^{III}-Fe^{III}$, $MMOH_{ox}$; $Fe^{II}-Fe^{III}$, $MMOH_{mv}$; $Fe^{II}-Fe^{II}$, $MMOH_{red}$),[17−19] high-resolution, diffraction-quality crystals of an MMOH−MMOB complex have been elusive. Spectroscopic studies on the interaction between MMOH and MMOB have determined that MMOB perturbs the ligand field of one of the Fe atoms in the diiron active site.[10] This interaction may allow O_2 to bind between the inequivalent Fe centers in a way that would activate the O−O bond for catalysis. The solution NMR structure of MMOB reveals that, if MMOB docks onto the "canyon region" of MMOH, the closest residues of MMOB would be >10 Å away from the buried diiron center in MMOH.[8] Thus, there is much interest in determining what structural effects MMOB might have on the active site of MMOH.

A protein closely related to MMO, but with different catalytic specificity, is toluene/*o*-xylene monooxygenase (ToMO).[2,20] ToMO belongs to a class of BMMs that includes phenol hydroxylase (PH) and other toluene monooxygenases (T4MO, T2MO, etc.).[2] ToMO, from *Pseudomonas stutzeri* OX1, has the ability to oxidize not only toluene and *o*-xylene, but a host of other arenes, alkanes, and haloalkanes.[21,22] Hydroxylases of MMO and ToMO (MMOH and ToMOH) have similar structures in the oxidized forms,[22] and like MMO, the ToMO protein system also contains a coupling protein, referred to as ToMOD.[2] It is of interest to compare the structure of the active site of ToMOH in the reduced form ($ToMOH_{red}$) to that of the well-characterized $MMOH_{red}$ to begin to unravel the differences in the reactivities of the two proteins. Furthermore, to understand these protein systems fully, determining whether the two coupling proteins MMOB and ToMOD play the same role and have similar effects on active site structure is of importance.

XAS is a technique well suited to examine both the geometric and electronic structural differences between the diiron sites in MMOH and ToMOH, as well as changes that might occur when MMOB/ToMOD is present in solution. The Fe K-edge and -preedge regions are used to investigate transitions from the 1s orbitals to the 3d, 4p, and continuum energy levels. Small changes in the covalency, coordination geometry, or ligand field of a metal site can often be detected by comparing these transitions for different samples.[23] The extended X-ray absorption fine structure (EXAFS) region of the XAS spectrum provides a means to determine the metal−ligand distances in an active site with sensitivity and accuracy.[24] Presented in this study is a comparison between the reduced active site structures of MMOH and ToMOH, alone and in the presence of their respective coupling proteins MMOB and ToMOD, by XAS.

Experimental Section

Protein Preparation. MMOH was purified from *Methylococcus capsulatus* (Bath) as previously described.[4,25] Purified MMOH contained 3.7−4.1 Fe atoms/dimer and catalyzed the epoxidation of propylene with a rate of 0.35 s^{-1} at 25 °C. MMOB was obtained from recombinant expression systems in *Escherichia coli* as described elsewhere.[26] ToMOH and ToMOD were purified as described.[22] ToMOH contained 3.8−4.2 Fe atoms/dimer and hydroxylated toluene at a rate of 6.1 s^{-1} at 25 °C. All proteins were exchanged into 25 mM MOPS, pH 7.0, and 20% glycerol and concentrated to make XAS samples containing ∼500−700 μM hydroxylase with and without two stoichiometric equivalents of the coupling protein (∼1000−1400 μM). Reduced samples contained 1 mM methyl viologen and 1−10 mM sodium dithionite and were prepared anaerobically. For each sample, ∼100 μL of sample solution, which was allowed to incubate for 10−20 min to complete the reduction, was transferred into a Lucite XAS cell with 37 μm Kapton tape windows and immediately frozen in liquid nitrogen.

Data Collection and Reduction. The X-ray absorption spectra for the $MMOH_{red}$ and $ToMOH_{red}$ samples were measured at the Stanford Synchrotron Radiation Laboratory (SSRL) on focused 16-pole wiggler beam line 9-3, with the ring operating at 3 GeV and 50−100 mA. A Si(220) monochromator was utilized for energy selection at the Fe K-edge. A harmonic rejection mirror was used to minimize higher harmonic components in the X-ray beam. The samples were maintained at 10 K during data collection using an Oxford Instruments CF1208 continuous flow liquid helium cryostat. Data were measured to $k = 15$ $Å^{-1}$ in fluorescence mode using a Canberra Ge 30-element array detector. Internal energy calibration was performed by simultaneous measurement of the absorption of an iron foil placed between two ionization chambers located after the sample. The first inflection point of the foil was assigned to 7111.2 eV.

No evidence of photoreduction was noted for any of the samples measured. The final averages included 31 scans for $MMOH_{red}$, 28 scans for $MMOH_{red}$ + MMOB, 33 scans for $ToMOH_{red}$, and 19 scans for $ToMOH_{red}$ + ToMOD.

The averaged data were processed by fitting a second-order polynomial to the postedge region and subtracting this background

(15) Lee, S.-K.; Nesheim, J. C.; Lipscomb, J. D. *J. Biol. Chem.* **1993**, *268*, 21569−21577.
(16) Liu, K. E.; Wang, D.; Huynh, B. H.; Edmondson, D. E.; Salifoglou, A.; Lippard, S. J. *J. Am. Chem. Soc.* **1994**, *116*, 7465−7466.
(17) Rosenzweig, A. C.; Frederick, C. A.; Lippard, S. J.; Nordlund, P. *Nature* **1993**, *366*, 537−543.
(18) Rosenzweig, A. C.; Nordlund, P.; Takahara, P. M.; Frederick, C. A.; Lippard, S. J. *Chem. Biol.* **1995**, *2*, 409−418.
(19) Whittington, D. A.; Lippard, S. J. *J. Am. Chem. Soc.* **2001**, *123*, 827−838.
(20) Bertoni, G.; Martino, M.; Galli, E.; Barbieri, P. *Appl. Environ. Microbiol.* **1998**, *64*, 3626−3632.
(21) Cafaro, V.; Izzo, V.; Scognamiglio, R.; Notomista, E.; Capasso, P.; Casbarra, A.; Pucci, P.; Di Donato, A. *Appl. Environ. Microbiol.* **2004**, *70*, 2211−2219.
(22) Sazinsky, M. H.; Bard, J.; Di Donato, A.; Lippard, S. J. *J. Biol. Chem.* **2004**, *279*, 30600−30610.
(23) Westre, T. E.; Kennepohl, P.; DeWitt, J. G.; Hedman, B.; Hodgson, K. O.; Solomon, E. I. *J. Am. Chem. Soc.* **1997**, *119*, 6297−6314.
(24) Cramer, S. P.; Hodgson, K. O. *Prog. Inorg. Chem.* **1979**, *25*, 1−39.
(25) Willems, J.-P.; Valentine, A. M.; Gurbiel, R.; Lippard, S. J.; Hoffman, B. M. *J. Am. Chem. Soc.* **1998**, *120*, 9410−9416.
(26) Coufal, D. E.; Blazyk, J. L.; Whittington, D. A.; Wu, W. W.; Rosenzweig, A. C.; Lippard, S. J. *Eur. J. Biochem.* **2000**, *267*, 2174−2185.

from the entire spectrum. A three-region spline of orders 2, 3, and 3 was used to model the smooth background above the edge. Normalization of the data was achieved by subtracting the spline and setting the edge jump to 1.0 in the postedge region. The resultant EXAFS data were k^3-weighted to enhance the impact of high-k data. Because of the signal-to-noise level, the EXAFS data were truncated at $k = 13$ Å^{-1} for $MMOH_{red}$, $ToMOH_{red}$, and $ToMOH_{red}$ + ToMOD and at $k = 11.5$ Å^{-1} for $MMOH_{red}$ + MMOB during the analysis.

Theoretical EXAFS signals $\chi(k)$ were calculated using FEFF (version 7.00)[27−30] and fit to the data using EXAFSPAK.[31] The experimental energy threshold, E_0 (the point at which $k = 0$), was chosen as 7130 eV and was allowed to vary by a common amount (ΔE_0) for all components within a given fit. The structural parameters that were varied during the refinements include the bond distance (R) and the bond variance (σ^2). The σ^2 parameter is related to the Debye−Waller factor, which is a measure of thermal vibration and static disorder of the absorbers and scatterers. Coordination numbers were systematically varied during the course of the analysis, but were not allowed to vary within a given fit.

The intensities and energies of the preedge features for all samples were quantified using the fitting program EDG_FIT.[31] All spectra were fit over several energy ranges (7108−7116, 7108−7117, 7108−7118, and 7108−7119 eV), with varied backgrounds to give nine fits per sample. Each preedge feature was modeled with pseudo-Voigt line shapes of a fixed 1:1 ratio of Lorentzian to Gaussian contributions. The backgrounds were chosen to give a best fit to the preedge area while reproducing edge features. Each fit was considered successful if it simultaneously reproduced the data and the second derivative of the data over the entire energy range. The total area is the sum of the areas of all preedge features, where the area is approximated by peak height multiplied by the full width at half-maximum, scaled by 100. Error was calculated by determining the standard deviation for peak heights and half-widths for each preedge feature from all successful fits.[23]

Results

XAS Comparison of $MMOH_{red}$ and $ToMOH_{red}$. 1. Iron K-Edges. An overlay of the Fe K-edge spectra of $MMOH_{red}$ and $ToMOH_{red}$, along with those of three model complexes, is shown in Figure 1. The diferrous models $(Et_4N)_2[Fe_2(salmp)_2]\cdot 2DMF$,[32] $[Fe_2(O_2CH)_4(BIPhMe)_2]\cdot 1.5CH_2Cl_2$,[33] and $[Fe_2(OBz)(et\text{-}HPTB)](BF_4)_2$[34] have iron atoms that are both 6-coordinate, one 5-coordinate and one 6-coordinate, and both 5-coordinate, respectively. As can be seen from the figure, the edge positions for the two proteins and three models are very similar, and small differences can be attributed to the different effective nuclear charge of the iron centers in each case.[35,36]

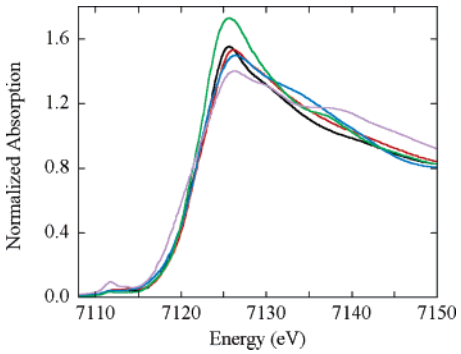

Figure 1. Fe K-edge data for $MMOH_{red}$ (black), $ToMOH_{red}$ (red), $(Et_4N)_2[Fe_2(salmp)_2]\cdot 2DMF$ (blue), $[Fe_2(OBz)(et\text{-}HPTB)](BF_4)_2$ (purple), and $[Fe_2(O_2CH)_4(BIPhMe)_2]\cdot 1.5CH_2Cl_2$ (green).

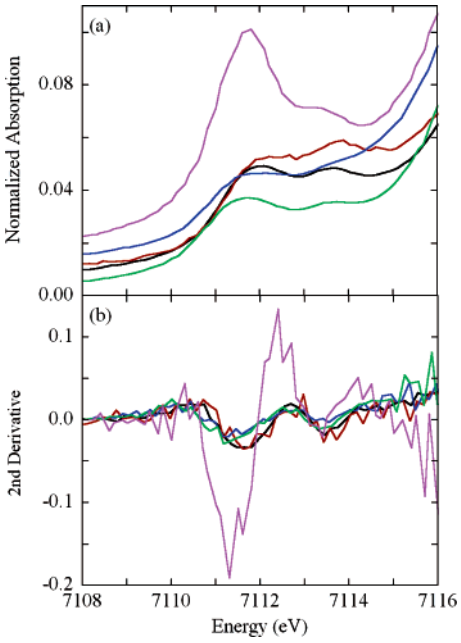

Figure 2. (a) Fe K-preedge data and (b) second derivatives for $MMOH_{red}$ (black), $ToMOH_{red}$ (red), $(Et_4N)_2[Fe_2(salmp)_2]\cdot 2DMF$ (blue), $[Fe_2(OBz)(et\text{-}HPTB)](BF_4)_2$ (purple), and $[Fe_2(O_2CH)_4(BIPhMe)_2]\cdot 1.5CH_2Cl_2$ (green).

An expansion of the 1s → 3d preedge transition areas and second derivatives of the normalized data of the Fe K-edges from Figure 1 are depicted in Figure 2. The quadrupole-allowed, but dipole-forbidden, transitions seen in the preedge area are sensitive to the coordination number of the Fe centers and to any distortions from centrosymmetry that increase the amount of 4p mixing into the 3d manifold.[23] From the overlay and fits to the data (Table 1), it is evident that the preedge transitions of $MMOH_{red}$ and $ToMOH_{red}$ are very similar in energy position, both proteins displaying transitions at 7111.9 and 7113.7 eV. The intensity distribution of the two peaks is, however, slightly different between the two. $MMOH_{red}$ has a more intense peak at lower energy, whereas the two peaks in the $ToMOH_{red}$ preedge are approximately equal in intensity. The total intensity of the two peaks is ∼10 units for both proteins, which may provide some information about the coordination environment of the

(27) Rehr, J. J.; Mustre de Leon, J.; Zabinsky, S. I.; Albers, R. C. *J. Am. Chem. Soc.* **1991**, *113*, 5135−5140.
(28) Mustre de Leon, J.; Rehr, J. J.; Zabinsky, S. I.; Albers, R. C. *Phys. Rev. B* **1991**, *44*, 4146−4156.
(29) Zabinsky, S. I.; Rehr, J. J.; Ankudinov, A.; Albers, R. C.; Eller, M. J. *Phys. Rev. B* **1995**, *52*, 2995−3009.
(30) Rehr, J. J.; Albers, R. C. *Rev. Mod. Phys.* **2000**, *72*, 621−654.
(31) George, G. N. EXAFSPAK & EDG_FIT, Stanford Synchrotron Radiation Laboratory, Stanford Linear Accelerator Center, Stanford University, Stanford, CA, 2000.
(32) Snyder, B. S.; Patterson, G. S.; Abrahamson, A. J.; Holm, R. H. *J. Am. Chem. Soc.* **1989**, *111*, 5214−5223.
(33) Tolman, W. B.; Bino, A.; Lippard, S. J. *J. Am. Chem. Soc.* **1989**, *111*, 8522−8523.
(34) Dong, Y.; Ménage, S.; Brennan, B. A.; Elgren, T. E.; Jang, H. G.; Pearce, L. L.; Que, L., Jr. *J. Am. Chem. Soc.* **1993**, *115*, 1851−1859.
(35) Kau, L.-S.; Spira-Solomon, D. J.; Penner-Hahn, J. E.; Hodgson, K. O.; Solomon, E. I. *J. Am. Chem. Soc.* **1987**, *109*, 6433−6442.
(36) Shulman, R. G.; Yafet, Y.; Eisenberger, P.; Blumberg, W. E. *Proc. Natl. Acad. Sci. U.S.A.* **1976**, *73*, 1384−1388.

Table 1. XAS Preedge Energies and Intensities for $MMOH_{red}$, $ToMOH_{red}$, $(Et_4N)_2[Fe_2(salmp)_2]\cdot 2DMF$, $[Fe_2(O_2CH)_4(BIPhMe)_2]\cdot 1.5CH_2Cl_2$, and $[Fe_2(OBz)(et\text{-}HPTB)](BF_4)_2$

sample	preedge peak energy	preedge peak intensity	total preedge peak intensity[a]
$MMOH_{red}$	7111.87 (0.05)	6.4 (0.9)	9.6 (0.8)
	7113.71 (0.10)	3.2 (0.5)	
$ToMOH_{red}$	7111.90 (0.05)	4.9 (0.6)	10.5 (0.9)
	7113.68 (0.06)	5.6 (1.2)	
$(Et_4N)_2[Fe_2(salmp)_2]\cdot 2DMF$[b]	7111.44 (0.04)	2.7 (0.2)	4.9 (0.3)
	7112.35 (0.07)	0.8 (0.3)	
	7113.57 (0.04)	1.4 (0.1)	
$[Fe_2(OBz)(et\text{-}HPTB)](BF_4)_2$[b]	7111.68 (0.01)	10.9 (0.2)	13.1 (0.3)
	7113.41 (0.01)	2.2 (0.1)	
$[Fe_2(O_2CH)_4(BIPhMe)_2]\cdot 1.5CH_2Cl_2$	7111.55 (0.06)	5.7 (0.7)	9.0 (0.5)
	7113.59 (0.05)	3.3 (0.8)	

[a] Values reported for the preedge intensity are multiplied by 100 for convenience. [b] Fits were previously reported in ref 22.

two Fe centers in each protein through comparison to model complexes with well-defined crystal structures.

The crystal structure of $(Et_4N)_2[Fe_2(salmp)_2]\cdot 2DMF$[32] shows that each Fe center is ligated by four oxygen and two nitrogen atoms at distances between 2.05 and 2.20 Å. This geometry is best described as distorted octahedral.[32] Fits to the preedge spectrum[23] (Table 1) of $(Et_4N)_2[Fe_2(salmp)_2]\cdot 2DMF$ indicate that three transitions are present, split by 0.9 and 1.2 eV, with a total intensity of 4.9 units. This type of fit is typical for both mono- and dinuclear high-spin ferrous complexes.[23] Because of the geometry of the Fe sites, there is very little 4p mixing into the 3d manifold and the total intensity of the preedge features is quite low.

A comparison of the spectra of $(Et_4N)_2[Fe_2(salmp)_2]\cdot 2DMF$ and $[Fe_2(OBz)(et\text{-}HPTB)](BF_4)_2$[34] shows the difference between the preedge transitions of 6- and 5-coordinate iron complexes, the total intensity of the 1s → 3d transitions of the latter being much higher than that of the former. Fits to the preedge of $[Fe_2(OBz)(et\text{-}HPTB)](BF_4)_2$ reveal two transitions at 7111.7 and 7113.4 eV with intensities of 10.9 and 2.2 units, respectively.[23] Both Fe centers in this complex are ligated by three N and two O donors and have approximately trigonal bipyramidal geometry.[34] This distortion from centrosymmetry along the *z*-axis allows for significant $4p_z$ mixing into the $3d_{z^2}$ orbital and accounts for the extra intensity in the peak at 7111.7 eV.

The complex $[Fe_2(O_2CH)_4(BIPhMe)_2]\cdot 1.5CH_2Cl_2$[33] was chosen to provide a geometric configuration that is intermediate between those of $(Et_4N)_2[Fe_2(salmp)_2]\cdot 2DMF$ and $[Fe_2(OBz)(et\text{-}HPTB)](BF_4)_2$. This complex has one 6-coordinate Fe center that is ligated by four O atoms and two N atoms and one 5-coordinate Fe center bound to three O and two N atoms. The 5-coordinate site is also weakly ligated by a third O atom at 2.74 Å. These sites are described as octahedral and distorted trigonal bipyramidal, respectively.[33] The preedge fit to $[Fe_2(O_2CH)_4(BIPhMe)_2]\cdot 1.5CH_2Cl_2$ (Table 2) reveals two peaks at 7111.6 and 7113.6 eV with a total intensity of 9.0 units. The latter value is midway between those for $(Et_4N)_2[Fe_2(salmp)_2]\cdot 2DMF$ and $[Fe_2(OBz)(et\text{-}HPTB)](BF_4)_2$ (4.9 and 13.1 units, respectively), which is what would be expected for an intermediate geometry, and the lower energy feature is slightly more intense than the one to higher energy.

Table 2. EXAFS Fit Results for $MMOH_{red}$[a]

fit no.		R (Å)	σ^2 (Å^2)	ΔE_0	F[b]
1	5 O/N[c]	2.13	0.0102	−2.50	0.11
	3 C	3.07	0.0089		
	1 Fe	3.30	0.0111		
	10 N/O−C	4.42	0.0141		
2	4 O/N[c]	2.11	0.0098	−3.13	0.091
	1 O/N[c]	2.47	0.0700		
	3 C	3.03	0.0071		
	1 Fe	3.29	0.0133		
	10 N/O−C	4.42	0.0143		
3	4.5 O/N[c]	2.11	0.0112	−3.40	0.079
	0.5 O/N[c]	2.47	0.0052		
	3 C	3.03	0.0074		
	1 Fe	3.29	0.0133		
	10 N/O−C	4.41	0.0140		
4	0.5 O/N[c]	1.98	0.0017	−3.06	0.072
	4 O/N[c]	2.14	0.0062		
	0.5 O/N[c]	2.67	0.0138		
	3 C	3.04	0.0089		
	1 Fe	3.29	0.0123		
	10 N/O−C	4.42	0.0144		

[a] Errors are estimated to be 25% for coordination numbers and 0.01−0.03 Å for distances. [b] Error (F) is defined as $F = [\sum k^6(\chi_{obsd} - \chi_{calcd})^2]/n$, where n is the number of data points. [c] Scatterers differing by $Z = \pm 1$ are not distinguishable by EXAFS analysis. The ordering O/N indicates that an oxygen atom was used to model the backscattering in the theoretical fit.

Comparison of $MMOH_{red}$ and $ToMOH_{red}$ to these three model complexes reveals that the two proteins are most similar to the mixed-coordination model $[Fe_2(O_2CH)_4(BIPhMe)_2]\cdot 1.5CH_2Cl_2$. All three samples display two features in the preedge region and have total intensities for these transitions of ∼10 units. The 7111.6 eV transition in the model complex is shifted to slightly lower energy than those in the protein samples (7111.9 eV for both $MMOH_{red}$ and $ToMOH_{red}$). It is not clear from this study what could cause this shift to higher energy in the proteins, but it is not unreasonable to expect that model complexes and proteins would have slightly different 1s → 3d transition energies. Therefore, although the Fe centers in $MMOH_{red}$ have been described as 5-coordinate,[11] the present results reveal that the sites may be better described as either one 5- and one 6-coordinate or as intermediate between 5- and 6-coordinate. This analysis agrees well with the crystal structure of $MMOH_{red}$,[19] which indicates an average distance of ∼2.25 Å if each Fe is considered 5-coordinate plus a longer associated ligand at ∼2.59 Å.

2. EXAFS Analysis. Overlays of the Fourier transforms (Figure 3) and EXAFS data (Figure 3, inset) reveal significant differences between the data of $MMOH_{red}$ and $ToMOH_{red}$. The intensity of the first-shell peak, although centered at approximately the same R value, is much lower in $MMOH_{red}$ compared to that for $ToMOH_{red}$. Furthermore, the outer-shell peak centered at ∼3 Å (non-phase-shift-corrected) for $ToMOH_{red}$ is shifted to a shorter distance for $MMOH_{red}$. Examination of the EXAFS waves of the two samples (Figure 3, inset) reveals a very similar beat pattern and amplitude out to ∼8.5 Å^{-1}, at which point the $MMOH_{red}$ wave dampens out, while that of $ToMOH_{red}$ remains strong and distinct.

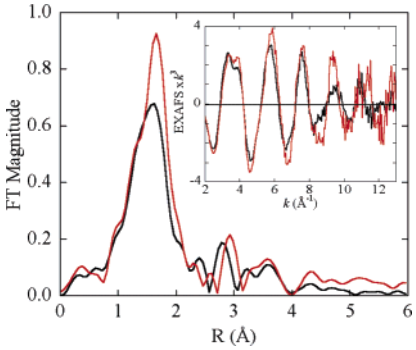

Figure 3. Non-phase-shift-corrected Fourier transforms (and EXAFS data, inset) for $MMOH_{red}$ (black) and $ToMOH_{red}$ (red). Note that the amplitude of the EXAFS data of $ToMOH_{red}$ stays strong to $k = 13$ Å^{-1}, while that of $MMOH_{red}$ decreases at $k = 9$ Å^{-1}.

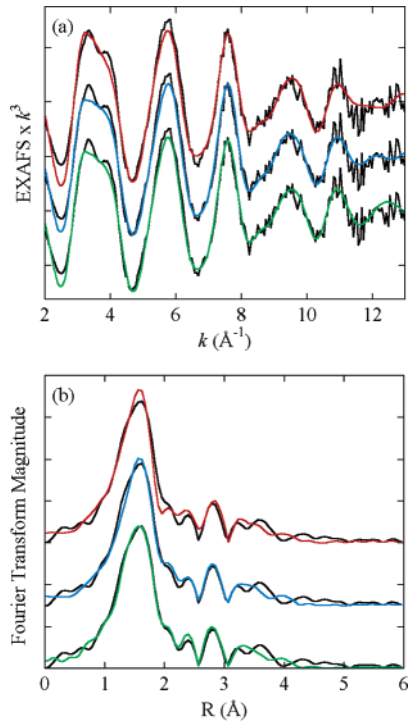

Figure 4. (a) EXAFS data (black) and (b) non-phase-shift-corrected Fourier transforms (black) for $MMOH_{red}$ and fit 1 (red), fit 3 (blue), and fit 4 (green) from Table 2.

Results of fits to the EXAFS data of $MMOH_{red}$ are presented in Figure 4 and Table 2. The initial fit (fit 1) includes five oxygen scatterers to model the first-shell O and N ligation from glutamate and histidine residues and the H_2O ligands present in the crystal structure active site. Also included in this fit are carbon scatterers at ~3 Å, an Fe scatterer at ~3.3 Å, and a group of long and relatively linear (140−160°) multiple scattering contributions from carbon and nitrogen atoms at ~4.4 Å. As can be seen in Figure 4, these scatterers provide a reasonable fit to the EXAFS data. The Fourier transform indicates, however, that a better fit may be possible if the five first-shell scatterers are divided into two or more components. Dividing the first shell into four medium (2.11 Å) and one long (2.47 Å) oxygen or nitrogen scatterer distances resulted in a very large σ^2 value for the long iron−oxygen path, but reduced the fit error from 0.11 to 0.091 (fit 2, Table 2). In fit 3, the coordination

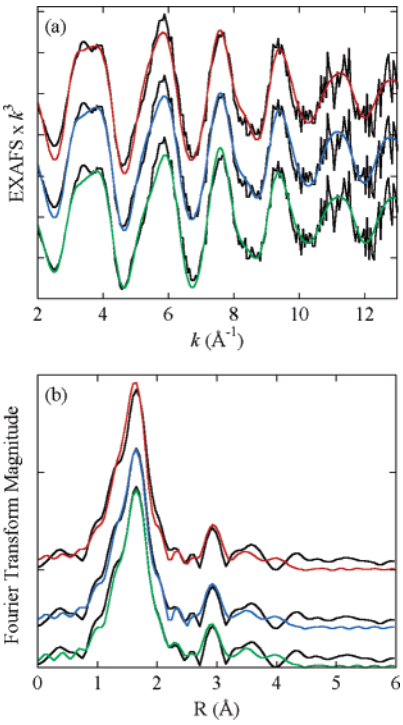

Figure 5. (a) EXAFS data (black) and (b) non-phase-shift-corrected Fourier transforms (black) for $ToMOH_{red}$ and fit 1 (red), fit 2 (blue), and fit 3 (green) from Table 3.

number of the longer O path was reduced to 0.5. The resulting fit (shown in blue in Figure 4) has a much lower error value compared to fits 1 and 2, and provides reasonable σ^2 values for all paths, and inspection of the Fourier transform indicates a better fit to the region between 2 and 3 Å. It is conceivable that an even better fit could be achieved by splitting the first-shell scattering into short, medium, and long paths. The result of such an attempt is fit 4 (shown in green in Figure 4), and although this fit is visually better than fit 1 or 3, scattering from 0.5 O atom at 2.67 Å would not be expected to contribute significantly to the total EXAFS wave. Thus, fit 3 is accepted as the most reasonable.

The fits to the EXAFS data of $ToMOH_{red}$ are given in Figure 5 and Table 3. As was the case when the $MMOH_{red}$ data were fitted, an initial fit (fit 1, shown in red in Figure 5) included five O/N, three C, one Fe, and five N/O−C scatterers. On the basis of the more pronounced low-*R* shoulder in the Fourier transform for $ToMOH_{red}$ (Figure 3), it was anticipated that this fit could also be improved by splitting the first-shell scattering into at least two components. Unlike $MMOH_{red}$, where a longer Fe−O path at ~2.5 Å improved the fit, no improvement occurred when such a component was included in the fits to $ToMOH_{red}$. A minor improvement was seen in the fit to the $ToMOH_{red}$ data by the addition of a shorter Fe−O path that fit to a distance of 1.96 Å with a coordination number of 0.5 (fit 2, shown in blue in Figure 5). Although the fit error was reduced only from 0.27 to 0.25 upon addition of this path, the visual quality of the fit improved in the first-shell region of the Fourier transform. A further attempt to split the first shell into short, medium, and long paths did not significantly improve the fit (fit 3, shown in green in Figure 5) and

Table 3. EXAFS Fit Results for ToMOH$_{red}$[a]

fit no.		R (Å)	σ^2 (Å^2)	ΔE_0	F^b
1	5 O/N[c]	2.12	0.0065	−2.00	0.27
	3 C	3.15	0.0154		
	1 Fe	3.41	0.0104		
	10 N/O−C	4.42	0.0103		
2	0.5 O/N[c]	1.96	0.0073	−2.81	0.25
	4.5 O/N[c]	2.12	0.0053		
	3 C	3.11	0.0220		
	1 Fe	3.41	0.0108		
	10 N/O−C	4.41	0.0100		
3	0.5 O/N[c]	1.98	0.0045	−3.44	0.23
	4 O/N[c]	2.12	0.0042		
	0.5 O/N[c]	2.53	0.0023		
	3 C	2.99	0.0383		
	1 Fe	3.41	0.0107		
	10 N/O−C	4.40	0.0097		

[a] Errors are estimated to be 25% for coordination numbers and 0.01−0.03 Å for distances. [b] Error (F) is defined as $F = [\sum k^6(\chi_{obsd} - \chi_{calcd})^2]/n$, where n is the number of data points. [c] Scatterers differing by $Z = \pm 1$ are not distinguishable by EXAFS analysis. The ordering O/N indicates that an oxygen atom was used to model the backscattering in the theoretical fit.

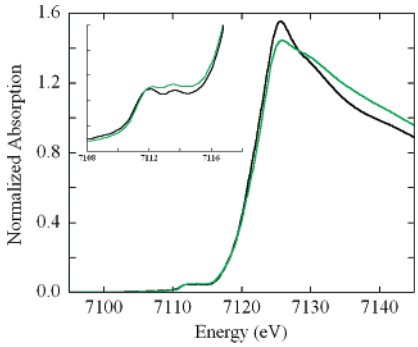

Figure 6. Fe K-edge data for MMOH$_{red}$, with (green) and without (black) MMOB. The inset shows magnification of the 1s → 3d preedge transition area.

exhibited strong correlation with the Fe−C wave. The first-shell coordination is therefore concluded to be 5-coordinate, most likely split into more than one distance, but for which the distribution cannot be firmly established given the resolution limitation imposed by the current k range of the data.

XAS Comparison of MMOH$_{red}$ versus MMOH$_{red}$ and MMOB. Figure 6 shows the effect of adding MMOB on the Fe K-edge of the reduced hydroxylase of MMO. Although there is very little difference in the preedge region and the position of the rising edge between the two samples, there is a significant difference in the spectra at energies greater than 7125 eV (Figure 6). The MMOH$_{red}$ spectrum has a sharp "white-line" maximum absorption feature that "decays" rapidly after the maximum, whereas that of MMOH$_{red}$ and MMOB is wider and falls off more slowly.

There are also small changes in the EXAFS data of MMOH$_{red}$ upon binding of MMOB (Figure 7, inset). The overall beat pattern of the protein data remains similar, but there is a slight shift in the EXAFS data at $k \approx 5$ Å^{-1} and a beat change at $k \approx 8.5$ Å^{-1} when MMOB is present. These differences are also seen in the Fourier transform comparison (Figure 7) between $R \approx 2$ Å and $R \approx 3$ Å. Using the best fit to MMOH$_{red}$ (Table 2, fit 3) as a starting point, the EXAFS data of MMOH$_{red}$ + MMOB were fit. These paths produced

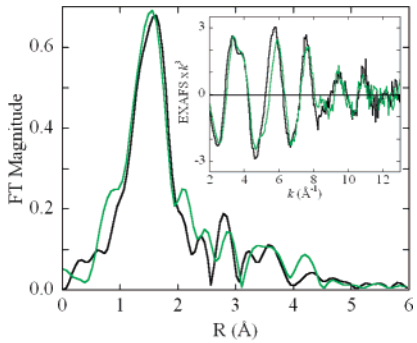

Figure 7. Non-phase-shift-corrected Fourier transforms (and EXAFS data, inset) for MMOH$_{red}$, with (green) and without (black) MMOB. Note the shift in the phase of the EXAFS data at $k = 5$ Å^{-1} when MMOB is present.

Table 4. EXAFS Fit Results for MMOH$_{red}$ + MMOB[a]

fit no.		R (Å)	σ^2 (Å^2)	ΔE_0	F^b
1	4.5 O/N[c]	2.10	0.0113	−3.79	0.12
	0.5 O/N[c]	2.48	0.0023		
	4 C	3.03	0.0109		
	1 Fe	3.31	0.0245		
	10 N/O−C	4.38	0.0157		
2	4.5 O/N[c]	2.09	0.0113	−4.55	0.083
	0.5 O/N[c]	2.48	0.0014		
	4 C	3.06	0.0073		
	1 Fe	3.24	0.0110		
	4 C	3.41	0.0100		
	10 N/O−C	4.36	0.0141		
3	4.5 O/N[c]	2.10	0.0113	−3.39	0.082
	0.5 O/N[c]	2.48	0.0030		
	4 C	3.05	0.0116		
	1 Fe	3.35	0.0179		
	8 O/N−C	4.04	0.0014		
	10 N/O−C	4.33	0.0143		
4	4.5 O/N[c]	2.09	0.0113	−4.51	0.070
	0.5 O/N[c]	2.48	0.0020		
	4 C	3.07	0.0097		
	1 Fe	3.30	0.0125		
	4 C	3.48	0.0193		
	8 O/N−C	4.04	0.0083		
	10 N/O−C	4.34	0.0114		

[a] Errors are estimated to be 25% for coordination numbers and 0.01−0.03 Å for distances. [b] Error (F) is defined as $F = [\sum k^6(\chi_{obsd} - \chi_{calcd})^2]/n$, where n is the number of data points. [c] Scatterers differing by $Z = \pm 1$ are not distinguishable by EXAFS analysis. The ordering O/N indicates that an oxygen atom was used to model the backscattering in the theoretical fit.

a reasonable fit to the EXAFS data, resulting in a well-modeled first-shell peak (Table 4, fit 1, Figure 8); however, the intensity in the Fourier transform between $R = 2$ Å and $R = 3$ Å was not well fit, and the σ^2 value for the Fe−Fe wave is high. This result indicated that scattering from light atoms (C, N, O) at longer distances (3.4−4.2 Å) would be necessary to provide a good fit. Such paths were not necessary in the fit to MMOH$_{red}$. Inclusion of four C scatterers at ∼3.4 Å (Table 4, fit 2) provided a better fit (reduction in the error value from 0.12 to 0.083), but the fit to the outer-shell peaks required further improvement. A similar decrease in error value was observed upon addition of a multiple scattering path to fit 1, resulting in fit 3 from Table 4. Despite the improvement, this fit was deemed unrealistic due to the low σ^2 value for the added path. Fit 4 contained a combination of both the single and multiple scattering paths from fits 2 and 3 and provided reasonable R and σ^2 values for all paths and a very good fit to the data.

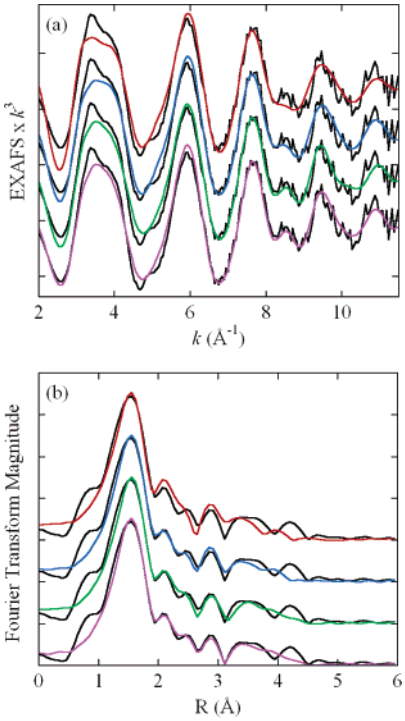

Figure 8. (a) EXAFS data (black) and (b) non-phase-shift-corrected Fourier transforms (black) for $MMOH_{red}$ + MMOB and fit 1 (red), fit 2 (blue), fit 3 (green), and fit 4 (purple) from Table 4.

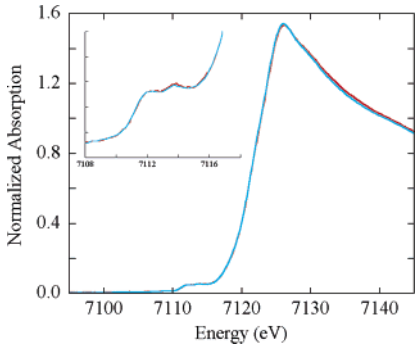

Figure 9. Fe K-edge data for $ToMOH_{red}$, with (light blue) and without (red) ToMOD. The inset shows magnification of the 1s → 3d preedge transition area.

Thus, the changes seen in the EXAFS data and subsequent Fourier transform when MMOB is present were due to changes in scattering contributions from outer-shell light atoms.

XAS Comparison of $ToMOH_{red}$ versus $ToMOH_{red}$ and ToMOD. Introduction of ToMOD to the $ToMOH_{red}$ sample had virtually no effect on the shape or energy position of the Fe K-edge or -preedge (Figure 9). There are minor differences between the Fourier transforms and EXAFS data (Figure 10) of the two samples. The most obvious change is the slight shift and change in intensity of the outer-shell peak centered at ~3 Å. Thus, it was expected that the same parameters that provided reasonable fits to the $ToMOH_{red}$ data would suffice for $ToMOH_{red}$ + ToMOD. Indeed, an excellent fit was found by the inclusion of five O/N, three C, and one Fe scatterers, as well as multiple scattering from N/O−C paths (fit 1 in Figure 11 and Table 5). Furthermore, splitting the first shell did not greatly reduce the error or

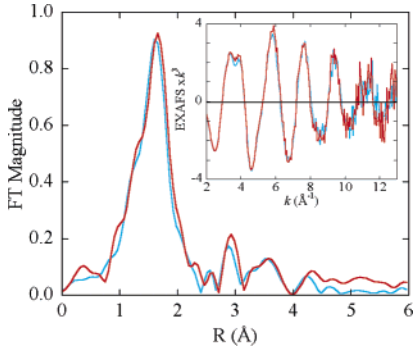

Figure 10. Non-phase-shift-corrected Fourier transforms (and EXAFS data, inset) for $ToMOH_{red}$, with (light blue) and without (red) ToMOD.

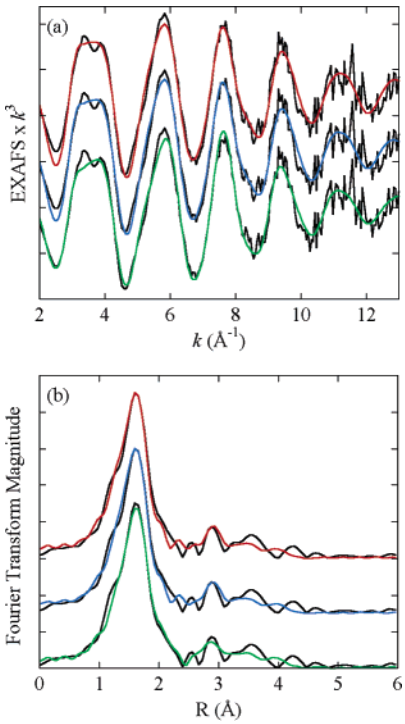

Figure 11. (a) EXAFS data (black) and (b) non-phase-shift-corrected Fourier transforms (black) for $ToMOH_{red}$ + ToMOD and fit 1 (red), fit 2 (blue), and fit 3 (green) from Table 5.

provide a visually much better fit (fits 2 and 3). One key difference between the two samples is found in the Fe−Fe vector. A small, but systematic, decrease in the Fe−Fe distance is found for $ToMOH_{red}$ + ToMOD (3.37 Å) compared to $ToMOH_{red}$ alone (3.41 Å). Although this smaller value is within the error limits typically quoted for EXAFS determinations, the difference was consistently obtained through more than 10 fitting approaches/models to each data set, and matches the difference in peak position in the Fourier transform. We therefore consider it to be significant. An increase in the σ^2 value for this path is also seen on binding of ToMOD.

Discussion

Comparison of $MMOH_{red}$ and $ToMOH_{red}$. The Fe K-edge spectra of $MMOH_{red}$ and $ToMOH_{red}$, when compared to those of selected model complexes,[32−34] reveal that the coordination numbers of the Fe sites in both proteins fall

Table 5. EXAFS Fit Results for ToMOH$_{red}$ + ToMOD[a]

fit no.		R (Å)	σ^2 (Å^2)	ΔE_0	F^b
1	5 O/N[c]	2.12	0.0071	−2.61	0.15
	3 C	3.12	0.0133		
	1 Fe	3.37	0.0145		
	10 N/O−C	4.41	0.0112		
2	0.5 O/N[c]	2.01	0.0026	−2.79	0.14
	4.5 O/N[c]	2.13	0.0059		
	3 C	3.12	0.0140		
	1 Fe	3.37	0.0150		
	10 N/O−C	4.40	0.0112		
3	0.5 O/N[c]	2.00	0.0021	−3.52	0.13
	4 O/N[c]	2.13	0.0050		
	0.5 O/N[c]	2.51	0.0031		
	3 C	3.01	0.0388		
	1 Fe	3.38	0.0181		
	10 N/O−C	4.39	0.0107		

[a] Errors are estimated to be 25% for coordination numbers and 0.01−0.03 Å for distances. [b] Error (F) is defined as $F = [\sum k^6(\chi_{obsd} - \chi_{calcd})^2]/n$, where n is the number of data points. [c] Scatterers differing by $Z = \pm 1$ are not distinguishable by EXAFS analysis. The ordering O/N indicates that an oxygen atom was used to model the backscattering in the theoretical fit.

between 5 and 6. The total preedge intensities for MMOH$_{red}$ and ToMOH$_{red}$ are ∼10 units, whereas typical dinuclear 6-coordinate and 5-coordinate Fe complexes have total intensities of ∼5 and ∼13 units, respectively.[23,32−34] It is possible, as in the case of the model complex $[Fe_2(O_2CH)_4(BIPhMe)_2]\cdot 1.5CH_2Cl_2$[33] studied here, that one Fe site is 5-coordinate while the other is 6-coordinate. Comparison to the crystal structure of MMOH$_{red}$,[19] however, indicates that a more probable explanation is that both Fe sites are 5-coordinate with a longer sixth ligand at an average distance between 2.5 and 2.7 Å. This sixth ligand would only be weakly associated with the metal at this distance, but could still influence the electronic structure of the metal, resulting in enough 4p mixing into the 3d manifold to see an increase in the total preedge intensity compared to that of octahedral 6-coordinate complexes. The redistribution in intensity of the two preedge transitions for MMOH$_{red}$ (6.4 and 3.2 units) and ToMOH$_{red}$ (4.9 and 5.6 units) is intriguing, but difficult to deconvolute, because both sites contribute to both preedge peaks. Thus, the intensity redistribution in the preedges of the two proteins could well reflect a small change in the active site of ToMOH$_{red}$ compared to MMOH$_{red}$ that may involve one or both Fe centers. This change, however, is not large enough to increase dramatically the 4p mixing into the 3d manifold in one protein over the other because the total intensities of the preedge transitions are about equal for the two proteins.

Analysis of the EXAFS spectra of MMOH$_{red}$ and ToMOH$_{red}$ provides additional insight into the differences in their active sites. The best fit to MMOH$_{red}$ included 4.5 O/N scatterers at 2.11 Å and 0.5 O/N scatterer at 2.47 Å. The average Fe−ligand distance found in the crystal structure of MMOH$_{red}$ is ∼2.25 Å for the five ligands closest to each Fe.[19] Thus, the EXAFS analysis gives a first-shell average distance that is ∼0.1 Å shorter than that of the crystal structure. This difference is reasonable given the resolution of the crystal structure and the differences between the two techniques.[19,37] The σ^2 value for the first-shell path is rather high (0.0112 Å^2) and indicates variable metal−ligand distance ligands around the Fe centers. This result agrees well with the crystal structure, which shows a range of distances, from 2.0 to 2.5 Å, for atoms bound to the Fe atoms. The average Fe−O/N distance found by X-ray diffraction for the mixed 5- and 6-coordinate Fe model discussed above is 2.11 Å,[33] whereas the 6- and 5-coordinate Fe models had average Fe−O/N bond lengths of 2.13 and 2.09 Å, respectively.[32,34] Thus, the EXAFS analysis correlates well to that of the edge, indicating that the Fe sites in MMOH$_{red}$ are intermediate between 5- and 6-coordinate.

The EXAFS spectrum and Fourier transform of ToMOH$_{red}$ reveal a scattering pattern very similar to that of MMOH$_{red}$. There are, however, several key differences in the two sets of spectra. The EXAFS beat envelope of MMOH$_{red}$ dies out at $k = 8.5$ Å^{-1}, as can be seen in the decrease in the EXAFS × k^3 signal from ∼2 at $k = 7$ Å^{-1} to ∼0.5 at $k = 9$ Å^{-1}. Conversely, the EXAFS beat envelope of ToMOH$_{red}$ remains strong out to $k = 10$ Å^{-1} (Figure 3). This difference is also reflected in the respective Fourier transforms, which display a much larger first-shell peak amplitude for ToMOH$_{red}$ versus MMOH$_{red}$. Although the need for a short-distance Fe−O/N ligand contribution, at 1.96 Å, in the fit to the first shell for ToMOH$_{red}$ is questionable, the σ^2 value for the first-shell short-distance contribution was consistently about half as large for this path in fits to ToMOH$_{red}$ as compared to MMOH$_{red}$. The ligands surrounding the Fe centers in ToMOH$_{red}$ are therefore less disordered than those in MMOH$_{red}$. Furthermore, the Fe−Fe distance in MMOH$_{red}$ is 3.29 Å, whereas that in ToMOH$_{red}$ is 3.41 Å. The less disordered first shell and longer Fe−Fe distance in ToMOH$_{red}$ compared to MMOH$_{red}$ may have important implications to the catalytic activity of the respective enzymes. MMOH is the only bacterial multicomponent monooxygenase that is capable of activating the inert C−H bond of methane,[1] which is probably a result of both access to the diiron active site and its structure. Recent X-ray crystallographic studies revealed a much larger opening from the surface to the diiron center in oxidized ToMOH as compared to oxidized MMOH.[22] Quenching of reaction intermediates by buffer components may be a consequence of this open access, in the absence of bound substrate, and may explain why intermediates have not been spectroscopically detected in pre-steady-state kinetic studies of the reaction of reduced ToMOH with dioxygen. Although XAS analysis is not sensitive to differences at the surface of the protein nor to residues far from the active site, there may be a correlation between a less disordered, more open active site, as found by EXAFS analysis, and the open access channel found in the X-ray structure of ToMOH. Further experiments are required to evaluate the reactivity differences between MMOH and ToMOH and how these relate to both the overall protein and active site structures.

Analysis of MMOH$_{red}$ and ToMOH$_{red}$, Alone and in the Presence of Coupling Proteins. Although no dramatic changes are seen electronically or geometrically upon binding of MMOB and ToMOD to their respective reduced hydrox-

(37) Freeman, H. C. In *Spectroscopic Methods in Bioinorganic Chemistry*; Solomon, E. I., Hodgson, K. O., Eds.; American Chemical Society: Washington, DC, 1998.

ylase proteins, the subtle changes observed by XAS may have important implications for a better understanding of the role of coupling proteins in the oxidation of hydrocarbon substrates by BMMs.

The present study reveals that, although the first-shell environment of $MMOH_{red}$ remains similar when MMOB is bound, the outer-shell residue scattering changes significantly. The requirement of light atom single and multiple scattering between 3.2 and 4.0 Å in the EXAFS fit to the $MMOH_{red}$ + MMOB data indicates that these residues are becoming more well ordered and are contributing to the overall EXAFS wave in a way that they do not when MMOB is absent. The ordering of amino acid residues may be correlated to the increased activity of MMOH when MMOB is present. MMOB may serve to "organize" the active site of the hydroxylase in the reduced state, allowing better control of O_2, methane, and possibly protons and/or electrons to the diiron center.

It has been documented that MMOB perturbs the ligand field on one Fe atom in the reduced form of the hydroxylase.[10] XAS probes the average environment of all Fe atoms present in the sample. Thus, a small change in the ligation of one Fe center may be difficult to detect in the EXAFS spectrum. This problem is further exacerbated here by the limited *k* range of the $MMOH_{red}$ + MMOB data. It can be stated, however, that although there is almost no change in the preedge transition area of the Fe K-edge when MMOB is present, a significant change in the shape of the Fe K-edge above ~7125 eV is apparent and is probably due to a change in the average electronic environment of the diiron active site.

The most significant change that occurred in the spectrum of $ToMOH_{red}$ when ToMOD was added, and which was not observed for $MMOH_{red}$ + MMOB, was a small change in the Fe−Fe separation. The σ^2 value for the Fe−Fe wave, however, is ~25% higher when ToMOD is present. This result could signify that ToMOD may work to allow the distance between the two Fe centers to be more flexible. Furthermore, no differences were observed in the outer-shell scattering contributions when ToMOD was present with ToMOH. These results may be correlated to the regiospecific hydroxylation observed in ToMO.[21] Further studies on these and other BMMs will allow better correlation of structure and reactivity.

Conclusions

Through the use of XAS Fe K-edge and EXAFS analysis the differences between two similar dinuclear iron monooxygenase proteins have been examined. The reduced active site in ToMOH is similar, but not identical, to the well-characterized site in reduced MMOH. Although only small electronic differences in the Fe K-preedge occur between the two proteins, interesting and significant differences were seen in the EXAFS region of the spectrum, including a more ordered first shell and a longer Fe−Fe separation for $ToMOH_{red}$. These differences may have important implications to the reactivity displayed by each protein. Furthermore, it has been shown in this study that MMOB and ToMOD, the coupling proteins of MMOH and ToMOH, respectively, have small effects on the dinuclear Fe active sites in the hydroxylases. The changes seen differ between the two proteins. In MMO, MMOB serves to "organize" the active site, which is observed in the EXAFS data through well-ordered outer-shell scattering when MMOB is present. ToMOD, in contrast, works to maintain a very well ordered first-shell environment around the Fe centers, but also seems to increase the flexibility of the Fe−Fe separation. This study thus provides a first step toward delineating not only the similarities and differences between different BMMs, but also the roles that the coupling proteins play in modifying active site structure and determining substrate specificity.

Acknowledgment. This work was supported by National Institutes of Health Grants GM-32134 (S.J.L.) and RR-01209 (K.O.H.). XAS data were measured at SSRL, which is supported by the Department of Energy, Office of Basic Energy Sciences. The Structural Molecular Biology program at SSRL is funded by the National Institutes of Health, National Center for Research Resources, Biomedical Technology Program, and the Department of Energy, Office of Biological and Environmental Research.

IC048794W